photonics

MDPI

Article

Coupled Cavity Mid-IR Quantum Cascade Lasers Fabricated by Dry Etching

Kamil Pierściński *, Dorota Pierścińska, Aleksandr Kuźmicz, Grzegorz Sobczak, Maciej Bugajski, Piotr Gutowski and Krzysztof Chmielewski

Institute of Electron Technology, Al. Lotników 32/46, 02-668 Warszawa, Poland; Dorota.Pierscinska@ite.waw.pl (D.P.); Aleksandr.Kuzmicz@ite.waw.pl (A.K.); Grzegorz.Sobczak@ite.waw.pl (G.S.); bugajski@ite.waw.pl (M.B.); gutowski@ite.waw.pl (P.G.); kchmielewski@ite.waw.pl (K.C.)

* Correspondence: kamil.pierscinski@ite.waw.pl; Tel.: +48-22-5487-937

Received: 27 May 2020; Accepted: 1 July 2020; Published: 3 July 2020

Abstract: In this work, two-section, coupled cavity, mid-IR quantum cascade lasers (QCLs) were characterized in terms of their tuning range and emission stability under operation towards potential application in detection systems. Devices were processed by inductively coupled plasma reactive ion etching (ICP-RIE) from InP-based heterostructure, designed for emission in the 9.x micrometer range. Single mode devices were demonstrated with a better than 20 dB side mode suppression ratio (SMRS). The fabrication method resulted in improved yield, as well as high repeatability of individual devices. Continuous, mode-hop-free tuning of emission wavelength was observed across ~4.5 cm^{-1} for the range of temperatures of the heat sink from 15 °C to 70 °C. Using the thermal perturbation in the lasing cavity, in conjunction with controlled hopping between coupled-cavity (CC) modes, we were able to accomplish tuning over the range of up to ~20 cm^{-1}.

Keywords: coupled cavity; quantum cascade lasers (QCLs); dry etching

1. Introduction

Quantum cascade lasers (QCLs) are compact laser sources of infrared radiation in the mid-IR range (3–20 μm) and in the THz range (1–5 THz). Their primary application is chemical spectroscopy [1], air quality monitoring [2], breath analysis for medical diagnostic [3], detection of explosives and dangerous substances [4,5] and industrial process monitoring [6]. One of the basic requirements for QCLs for these applications is a single mode emission spectrum. Typical QCLs based on the Fabry–Perot (FP) resonator are characterized by multi-mode emission [7], especially at higher operating currents. Since the first demonstration of the single mode QCL laser [8], several solutions have been proposed to achieve single mode emission. The most common are distributed feedback (DFB) [9] lasers and external cavity lasers [10]. There are also extremely short FP lasers (<200μm) [11], distributed Bragg reflector (DBR) [12] lasers and photonic crystals lasers [13]. However, these solutions have many limitations, mainly in terms of fabrication process, high cost and complicated, time-consuming processing. On the other hand, the external cavity lasers, which show the wavelength tuning range far better than that of DFB and DBR lasers, are bulky, vibration sensitive and more expensive compared to other solutions [14].

In this article an alternative approach to achieving single mode emission is presented: coupled-cavity quantum cascade lasers (CC-QCLs). The concept of coupled cavity lasers has been well-known since the early 1980s, especially from the works of Coldren et al. [15–17]. It has also been applied in the case of QC lasers [18]. However, despite the demonstrated feasibility of obtaining single mode operation of QCL by exploiting the coupled cavity approach, it has not been widely studied or

applied on a greater scale for device fabrication. The CC-QCLs reported so far were fabricated by a combination of dry and wet etching [19,20], cleaving the laser ridge [21] or FIB etching [18], which by the nature of the technique cannot be used to provide high throughput and low cost. The process developed in this work to fabricate devices is based exclusively on dry etching. It allowed the achievement of high throughput and high yield without further complications to standard QCL fabrication procedure. The results presented in this work are not unique—we have obtained SM operation of all of the working devices on the processed wafer. The paper focuses on technology and characterization of monolithic, coupled cavity two-section quantum cascade lasers for potential applications in gas detection systems. The devices were fabricated by reactive ion etching from InP-based heterostructure, designed for emission in 9.x micrometer range. We have previously presented CC-QCLs fabricated by means of focused ion beam (FIB) post-processing [22–24]. However, despite the advantages of FIB etching, it can hardly be considered as production technology because it is time-consuming and of inherently low throughput. In this work, in order to overcome the disadvantages of the FIB process, gaps separating sections were defined by dry etching during the fabrication process [15]. Furthermore, it is shown directly how the FTIR (Fourier transform infrared) spectrum of pulsed operated lasers becomes broadened due to in-pulse shift of the emission wavelength even for short (hundreds of ns) pulses.

2. Investigated Devices and Fabrication Technology

The investigated devices were AlInAs/InGaAs/InP lattice matched QCLs, grown by molecular beam epitaxy (MBE) technology, designed for emission at ~9.2 μm [25]. The QCL structures were grown using lattice-matched $In_{0.53}Ga_{0.47}As/In_{0.52}Al_{0.48}As$ active region of four-well two-phonon resonance design. The layer sequence of one period of the structure, in nanometers, starting from the injection barrier, was 4.0, 1.9, 0.7, 5.8, 0.9, 5.7, 0.9, 5.0, 2.2, 3.4, 1.4, 3.3, 1.3, 3.2, 1.5, 3.1, 1.9, 3.0, 2.3, 2.9, 2.5, 2.9 nm. The AlInAs layers were denoted in bold. The underlined layers were *n* doped to 1.5×10^{11} cm^{-2}. The waveguide from the bottom side was formed by a low doped InP substrate and from the top by a 2.5 μm $In_{0.52}Al_{0.48}As$ layer covered by a heavily doped $In_{0.53}Ga_{0.47}As$ layer [26].

Fabrication of CC-QCL by dry etching requires slight modification of the standard fabrication process of double trench waveguide QCL [27]. A schematic illustration of device fabrication process is shown in Figure 1. The optical gap of specified width (of about 9 μm) was dry etched simultaneously with mesa (ridge), and the depth of the etch was ca. 9 μm. First, a robust dielectric mask was prepared by the PECVD (plasma enhanced chemical vapor deposition) method to protect a defined area of the sample. Second, deep etching in RIE ICP (reactive ion etching, inductively coupled plasma) methane–hydrogen–chlorine–argon gas mixture plasma (Plasmalab System 100 RIE ICP, Oxford Instruments) of the processed heterostructure was employed in order to obtain a close to anisotropic etch profile. A mechanical stress-compensated Si_3N_4 dielectric thin film was prepared by the PECVD method, and contact windows were plasma etched in a CHF_3/SiF_6 reactive gas mixture (RIE ICP). The electrical gap width was defined by photolithography for metallization lift-off. The following types of metallization were used: Ti/Pt/Au as the top contact at the epi-side and AuGe/Ni/Au at the substrate side of the laser structure. The contact pads were thickened by galvanic gold electrodeposition from basic solution to improve heat dissipation. Just before bottom contact magnetron sputtering, the QCL structure was chemo-mechanically (CM) thinned down to around 150 μm. The front and back sections of the slot QCL were electrically separated by a 100 μm gap in the Ti/Pt/Au top contact layer. RTA (rapid thermal annealing) in inert atmosphere (to decrease characteristic contact resistance) was employed to finalize the QCL processing [28].

After processing, the lasers were cleaved into the 2-mm-long cavities and In-soldered, epi-side up, on a gold coated copper mount and wire bonded. Figure 2 shows an optical microscope image of a part of processed epitaxial wafer (a), close up on a single chip of CC-QCL (b) and close up on a dry-etched optical and electric gap (c–d). The investigated CC-QCLs had a short section (SS) of 400 μm and a long

section (LS) of 1600 μm. The width of the air gap was 9.2 μm, which was equal to the free-space λ (emission wavelength of the device).

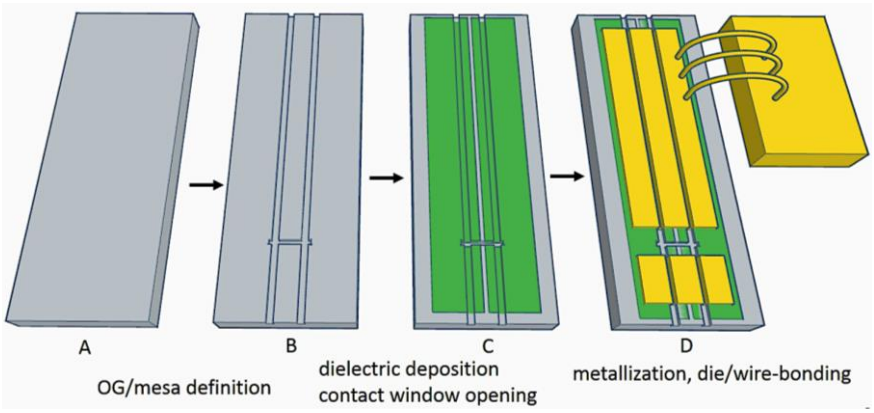

Figure 1. Schematic drawing of the fabrication process for the dry-etched CC-QCL.

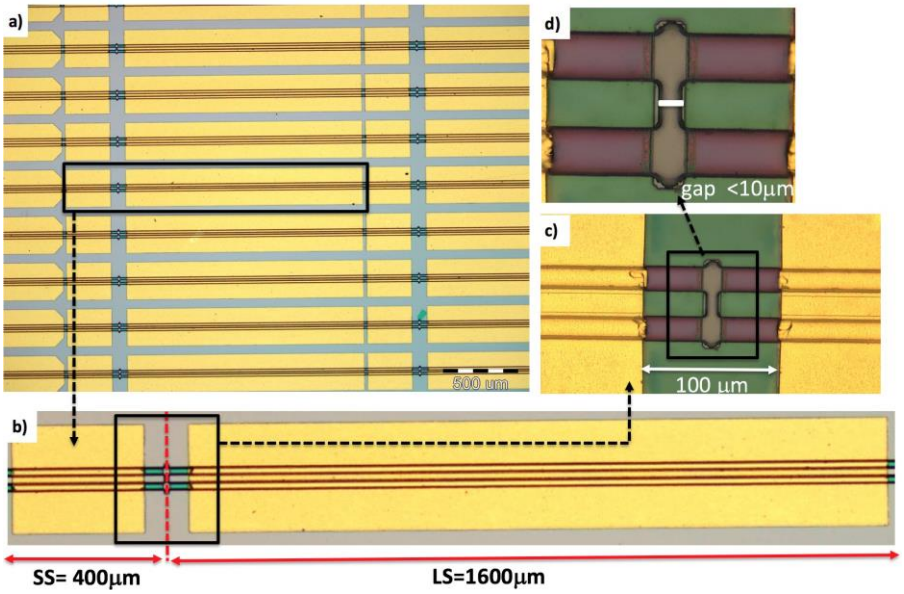

Figure 2. Optical microscope image of a part of processed epitaxial wafer of CC-QCL (**a**), close up on single chip (**b**) and close up on dry-etched optical-electric gap (**c**,**d**).

To minimize scattering losses and provide efficient coupling between two sections of QCL a special effort was devoted to reducing roughness of sidewalls of waveguides and to provide close to 90-degree sidewall angles of the slot. Scanning electron micrograph (SEM) images of fabricated CC-QCL, shown in Figure 3, confirm that smooth sidewalls were achieved (Figure 3b,c). Additionally, a laser scanning confocal microscope image of the slot area showed the sidewall angle of about ~95 degrees and acceptable roughness of sidewalls (Figure 3d).

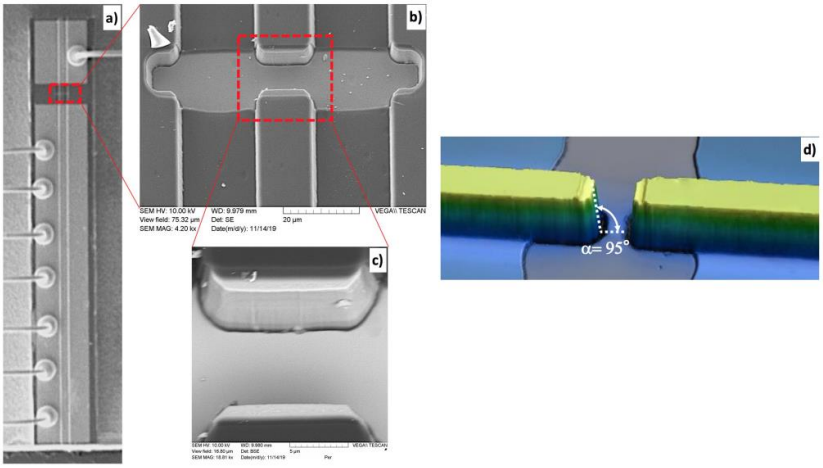

Figure 3. SEM images of dry-etched fabricated CC-QCL with close up on dry-etched optical gap. The whole device (**a**), close-up on the dry-etched optical gap (**b**,**c**). Laser scanning confocal microscope image of the gap (**d**).

3. Experimental Results and Discussion

The investigated CC-QCLs with dry-etched gap (shown schematically in Figures 1–3) were placed on a temperature stabilized heatsink, including a thermistor and thermo-electrical-cooler (TEC), to stabilize the temperature. The temperature of the device was kept at 20 °C for all light–current–voltage (L–I–V) measurements. The L–I–V measurements were performed in a standard experimental set-up [29] with a TE-cooled mercury–cadmium–telluride (MCT) detector. The emission measurements were performed using a Fourier transform infrared (FTIR) spectrometer (Nicolet 8700) with a liquid-nitrogen cooled photovoltaic MCT infrared detector placed inside the spectrometer. The spectral resolution of the spectrometer was 0.125 cm^{-1}. The time resolved spectral (TRS) measurements were performed with 5 ns time resolution [30]. For all measurements, the LS of the QCL was driven by power supply. The SS was not biased, acting as a passive filter.

Figure 4 shows L–I–V characteristics of investigated CC-QCLs with different active area width: 9.4 µm, 14.5 µm, 19.5 µm. Figure 4a shows emitted optical power and voltage vs. current (L–I–V curves). Figure 4b shows emitted power and voltage vs. current density. It can be observed that the threshold current for all investigated devices is reached at the same voltage equal to V_{th} = 8 V. With the increase of the ridge width, the amount of emitted optical power increases, which is connected with larger volume of active region. The observed increase of the threshold current density with decrease of ridge width is connected with increased contribution of waveguide sidewall scattering losses. In each case, only the long section was biased with 200 ns pulses at 5 kHz repetition rate. The optical emission was collected from the side of long section.

Figure 5a shows comparison of L–I–V characteristics of the investigated CC and FP devices fabricated from the same epitaxial wafer as the reference sample. The lasers were driven in pulse mode with pulse width of 200 ns and repetition rates of 5 kHz. In the case of CC-QCL, only the long section was driven by 200 ns/5 kHz pulses and the short section was unbiased. The measured threshold current density of CC-QCL was higher (~1.03 times) than for reference FP QCL, which seems to be reasonable when taking into account increased losses due to shorter cavity and the etched mirror on the gap side. The dimensions of active region of the reference FP QCL were as follows: width 14.5 µm and length 2 mm. The optical output power for CC-QCL collected from a single facet exceeded 95 mW at room temperature, which was approximately 3.5 times lower than for FP QCL.

Figure 5b shows emission spectra of CC and FP devices registered for the same current density of 7.3 kA/cm^2 at room temperature. Both the FP device and the long section of CC-QCL were operated in pulse mode with a pulse width of 200 ns and 5 kHz repetition rates. A single mode operation of CC-QCL was obtained at ~1098.05 cm^{-1}. The full width at the half maximum (FWHM) of the mode was equal to 0.5 cm^{-1},

as extracted from spectra measured with FTIR with 0.125 cm^{-1} resolution. Both spectra overlapped, with the CC-device emission in the range of the FP device emission. Single mode emission spectrum of fabricated CC-QCL showing side mode suppression ratio (SMSR) equal to 27 dB is shown in Figure 6.

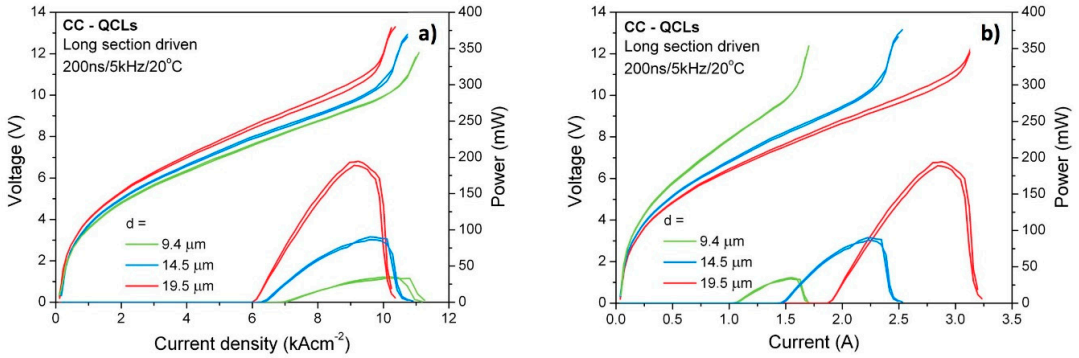

Figure 4. L–I–V curves of reactive ion etching (RIE) fabricated CC-QCLs with different active area width: 9.4 μm (green line), 14.5 μm (blue line), 19.5 μm (red line). Light-voltage curves vs. current (**a**), Light-voltage curves vs. current density (**b**).

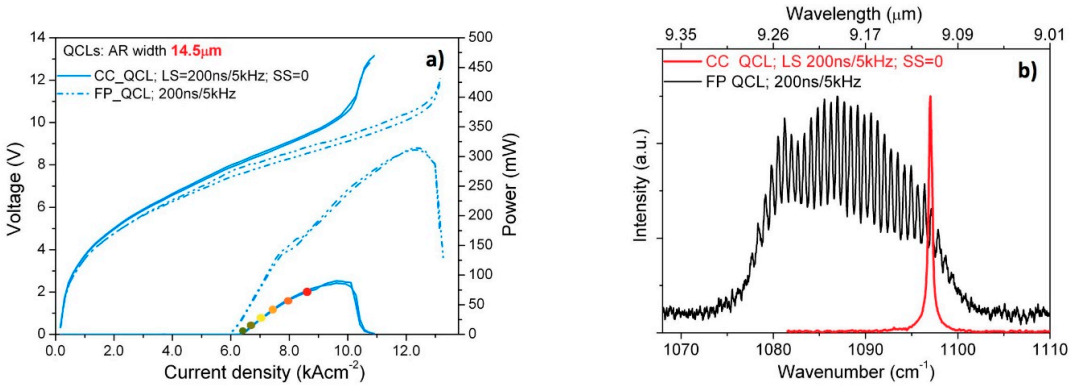

Figure 5. Comparison of L–I–V curves of RIE fabricated CC-QCLs (solid line) and FP QCL (dash-dot line) (**a**); comparison of emission spectra of CC-QCL and FP QCL at the constant current density/the same values of supplied current density 7.3 kA/cm^2 (**b**).

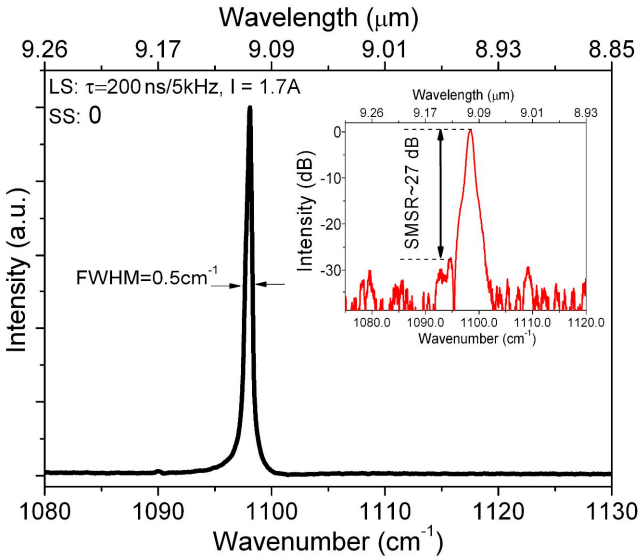

Figure 6. Room temperature single mode emission spectrum of RIE fabricated CC-QCL. The laser was driven with 1.7 A current applied to the long section. The short section was unbiased.

To illustrate the tuning behavior, the optical spectra were registered in case of current tuning and temperature tuning by external heating, as well as time resolved spectra during the pulse for increasing duty cycle (increasing thermal load).

3.1. Temperature and Current Tuning of CC-QCL

A continuous tuning of the coupled cavity modes can be realized through an index perturbation of the lasing cavity by control of either the injected current or heat sink temperature. Figure 7 presents standard temperature tuning results. The temperature of the device was changed externally by the TEC element, stabilizing the temperature of the heatsink of the device. As shown in Figure 7, the wavelength shifted continuously, without mode hops, and tuned across ~4.5 cm^{-1} for the range of temperatures of the heat sink from 15 °C to 70 °C. SMSR decreased from 27 dB to 22 dB when the heat sink temperature was increased (see inset in Figure 7). As the current was increased, a gradual increase of the spectrum width could be observed. It was connected with thermal tuning of emission during pulse at higher currents. This effect will be discussed in a subsequent section in the context of intrapulse tuning.

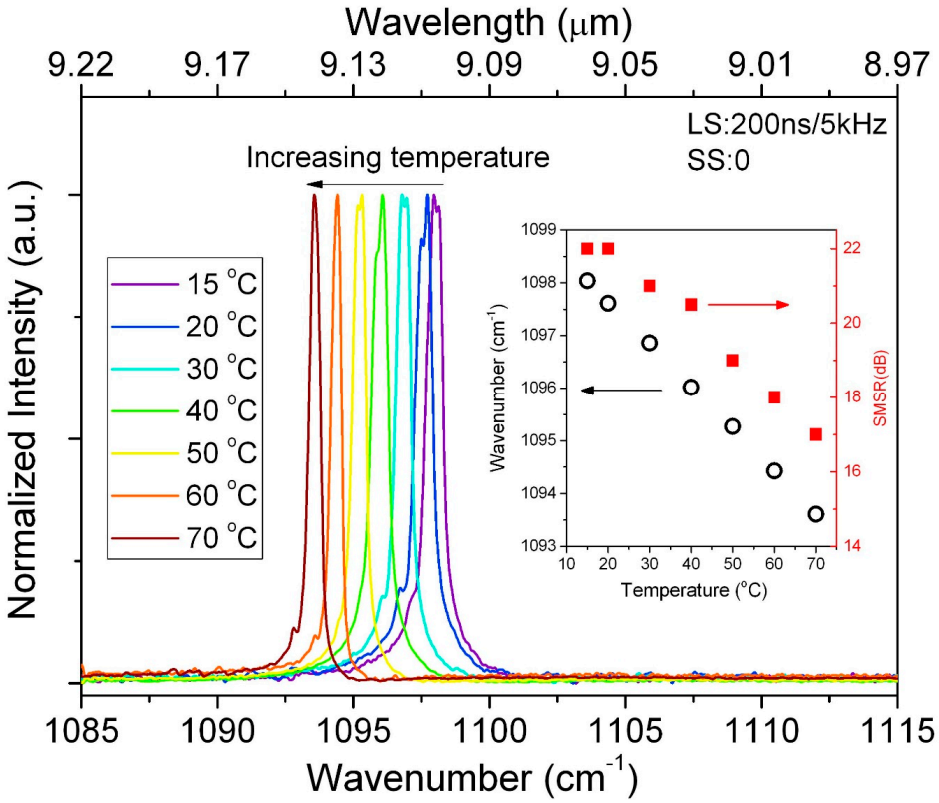

Figure 7. Emission spectra of the CC-QCL operated at the constant current level I = 1.15 I_{th} and various heat sink temperatures. Inset shows the single mode emission wavenumber and side mode suppression ratio (SMSR) vs. heat sink temperature.

Figure 8 shows emission spectra of CC-QCL, registered at different operating points on the L-I characteristics of the device shown in Figure 5a. The device was operated in pulse mode with 200 ns pulses and 5 kHz repetition rate with the short section unbiased. The stable single mode operation from the threshold current of ~1.48 A up to ~2.00 A (L–I rollover point) was registered. The slight shift of the emission towards longer wavelength with increasing current is due to the self-heating of the device.

3.2. Intrapulse Tuning of CC-QCL

One of the tuning schemes used in sensing techniques based on laser absorption spectroscopy is intrapulse tuning. In this technique, the emission wavelength is tuned across the range of wavelengths during a pulse of supply current. This technique has the advantage of measuring rapidly changing gas concentrations, which is the case with combustion and plasma processes. The rise of the temperature during the pulse results in the shift of emission towards longer wavelengths (red-shift). To verify how CC devices would perform in an intrapulse sensing scheme, time-resolved spectra (TRS) of emission of CC devices were registered. The time-resolved FTIR measurements of pulsed operated QCL were measured with a 0.125 cm^{-1} spectral resolution and 5 ns time resolution [30]. Figure 9 presents a wavelength and time resolved map, showing the evolution of the spectrum during the pulse. The measurement was performed at room temperature (laser temperature stabilized at 20 °C) for the device operated with 200 ns pulses at 5 kHz repetition rate. The device emitted in a stable, single mode throughout the pulse. During the 200 ns pulse, the wavelength shifted by $\Delta\lambda = 1.02$ cm^{-1}. The shift of wavelength is even better visualized in Figure 10a presenting normalized spectra extracted from the map in Figure 9.

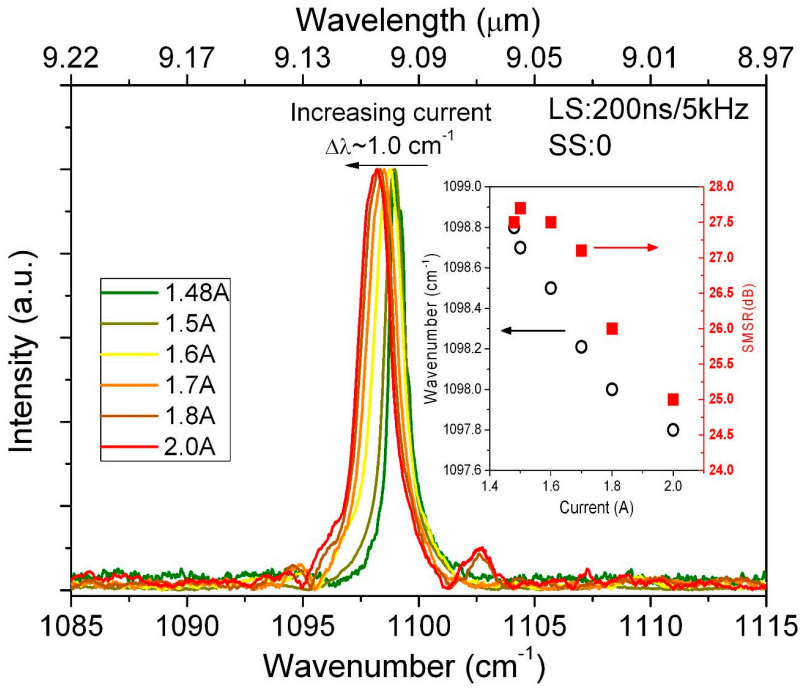

Figure 8. Emission spectra for RIE fabricated CC-QCL for currents starting at the threshold current 1.48 A (6.4k A/cm^2) up to 2.0 A (8.6 kA/cm^2). Device operated in pulse mode with pulse width 200 ns and repetition rates 5 kHz, with the short section unbiased. The color coding of individual spectra refers to particular points on L–I characteristics, as indicated in Figure 5a.

Spectra at different time delays within the pulse showed a thermal shift due to a temperature rise in the laser core during the current pulse. The arrow indicates the direction of the shift of the lasing wavelength. Spectral tuning towards lower energy was observed, i.e., a red-shift connected with temperature induced a change of the effective refractive index of the active region [31]. Here, a wavelength shift $\Delta\lambda = 1.02$ cm^{-1} was clearly visible. Figure 10a presents normalized spectra composing the map from Figure 9, showing clearly the shift of emission wavelength. Spectra in Figure 10b show the evolution of the intensity of the optical spectrum during the pulse. It thus becomes apparent that spectra registered with FTIR normal mode of operation (so called rapid scan—RS) will appear broadened. The black line in Figure 10b was registered in rapid scan mode of FTIR. It is apparent that this spectrum was an envelope of the spectra recorded in TRS mode (shown in the figure

in color). The RS spectrum can be thought of as a sum of the individual spectra (registered at time steps) forming the map shown in Figure 9. This behavior was due to the dynamic heating and cooling with respect to the current pulse, which resulted in a temporal variation of the refractive index.

Additional measurements were performed for longer pulses and higher repetition rates to verify how increased duty cycle influenced the spectra of CC-QCL. Figure 11 shows the L–I–V characteristics for CC-QCL operated in pulse mode with 1 μs pulses and repetition rate of 5 kHz. As in previous measurements, only the long section was driven and the short section was left unbiased. As compared to 200 ns/5 kHz operating conditions, the threshold current density was 1.54 kA/cm^2, which was slightly higher (~1.03 times), and the optical output power was about 60 mW.

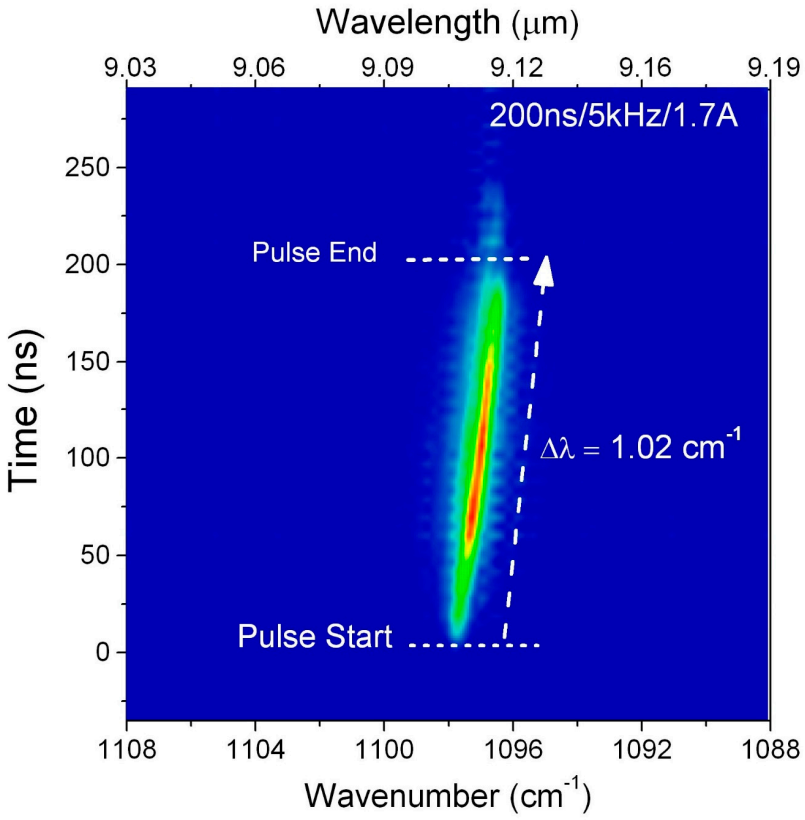

Figure 9. Time-resolved map of emission of CC-QCL operated with 200 ns pulses at 5 kHz repetition rate.

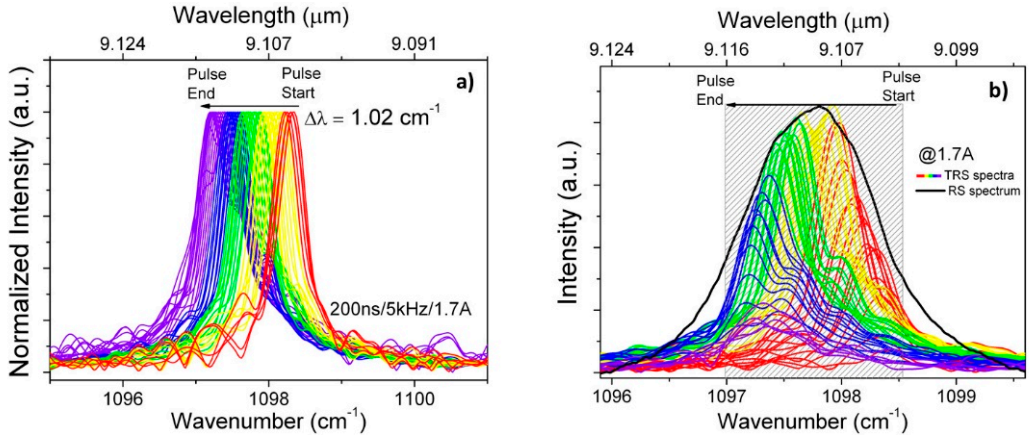

Figure 10. Normalized (**a**) and non-normalized (**b**) emission spectra extracted from the time resolved map registered for CC-QCL operated with 200 ns pulses at 5 kHz repetition rate. The black line presents the spectrum recorded in rapid scan mode of FTIR at the same experimental conditions.

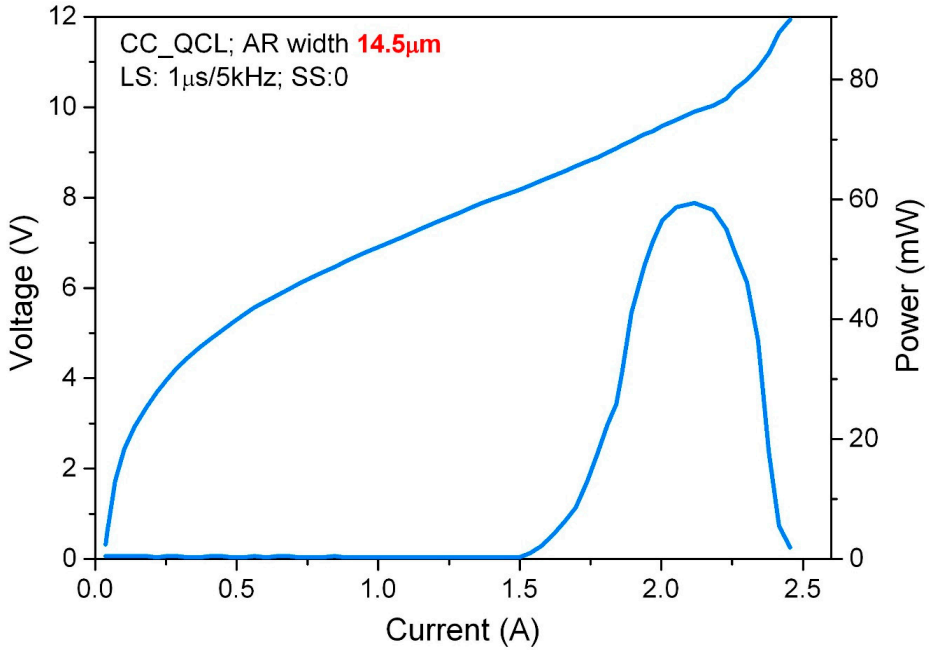

Figure 11. L–I–V curves of CC-QCL. The long section is driven in pulse mode with 1 μs pulses and repetition rate 5 kHz. The short section is unbiased.

In gas spectroscopy, the fine tuning of the emission frequency of a laser system is required to shift the probe wavelength over a specific absorption line of investigated molecule [32]. This can be achieved by application of longer current pulses producing heating of the active region of the laser. Figure 12a shows emission spectra vs. current of CC-QCL operated in pulse mode with pulse width equal to 1 μs and repetition rate of 5 kHz. The single mode operation was registered only near the threshold current of ~1.52 A. With the increase of the current, additional modes appeared in the spectra [33]. Distance between additional modes equaled 8 cm^{-1}. Figure 12b shows emission spectra of CC-QCL registered at different repetition rates in the range from 5 kHz to 50 kHz.

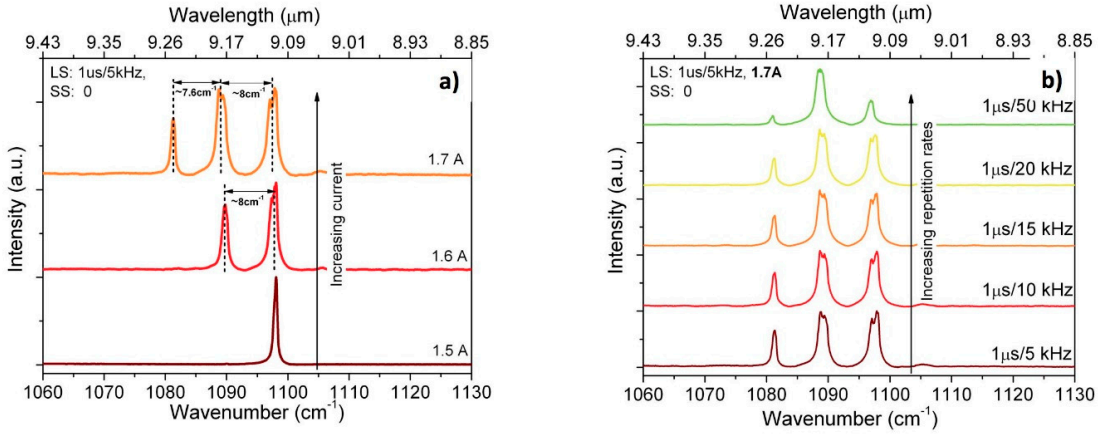

Figure 12. Emission spectra of CC-QCL registered for a set of currents starting at the threshold current of 1.5 A (6.5 kA/cm^2) up to 1.7 A (7.3 kA/cm^2) (**a**); emission spectra for CC-QCL for a set of repetition rates in the range from 5 kHz to 50 kHz (**b**). Device was operated in pulse mode with pulse width of 1 μs. The short section was unbiased.

The nature of the observed mode hopping between adjacent laser modes is more visible in Figure 13a, which presents a time resolved map of emission for CC-QCL. It can be seen that during the pulse, the instantaneous emission was single mode, although with time, the emission wavelength hopped abruptly to the next allowed resonances of the coupled-cavity system. Figure 13b presents

spectra extracted from the map at different delay times with respect to current pulse. A thermal shift in wavelength due to the rise in core temperature during the pulse occurred, resulting in the continuous tuning of ~1.3 cm^{-1} of each of the modes. The shift in the last group of modes was smaller (0.5 cm^{-1}), due to the drop of the power by the end of the pulse, associated with thermal rollover reducing the laser emission.

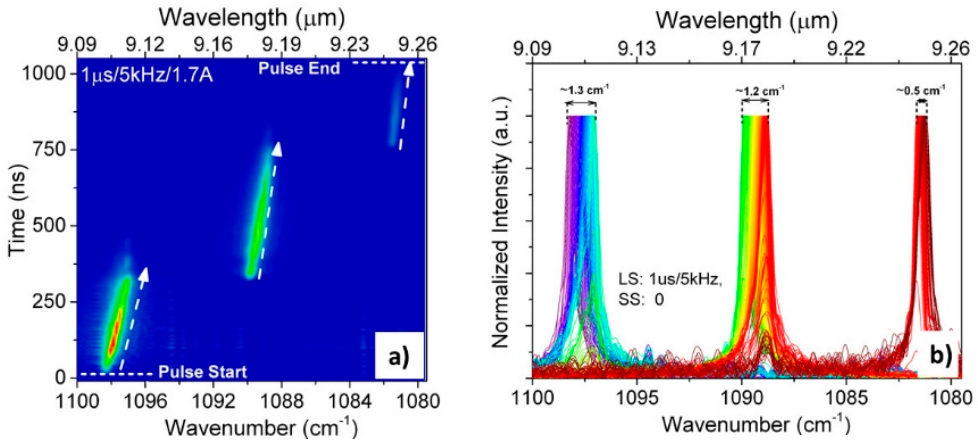

Figure 13. Time-resolved map (**a**) and normalized emission spectra extracted from the map (**b**), registered for CC-QCL operated with 1 μs pulses at 5 kHz repetition rate.

Using the thermal perturbation in the lasing cavity, in conjunction with controlled discrete frequency tuning between CC modes, we were able to accomplish tuning over the range of up to ~20 cm^{-1} while maintaining SMSR better than 20 dB.

4. Conclusions

In this work we presented the fabrication and characterization of the coupled-cavity QCLs towards their potential application in detection systems. Devices were fabricated by ICP-RIE from InP-based heterostructure, designed for emission in 9.x micrometer range. The technology scheme used to fabricate coupled cavity lasers allows high repeatability and yield. Single mode devices were obtained, exhibiting a side mode suppression ratio of more than 20 dB. Continuous, mode-hop-free tuning of emission wavelength was observed across ~4.5 cm^{-1} for the range of temperatures of the heat sink from 15 °C to 70 °C. Using the thermal perturbation in the lasing cavity, in conjunction with controlled hopping between CC modes, we were able to accomplish a tuning over the range of up to ~20 cm^{-1}. The evolution of the spectrum during the pulse was registered using time-resolved FTIR measurements, at the same time providing unbroadened spectra as compared to standard rapid or step-scan modes.

Author Contributions: Conceptualization, methodology, data analysis, drafting, and writing of the manuscript, K.P.; characterization of devices D.P., K.P. and G.S.; review and editing of the manuscript M.B.; structure growth, P.G.; fabrication of devices, A.K. and K.C. All authors discussed results and contributed to the formulation of conclusions. All authors have read and agreed to the published version of the manuscript.

Funding: This work was supported by National Center for Research and Development (Poland) by project TECHMATSTRATEG: SENSE no. 1/347510/15/NCBR/2018.

Conflicts of Interest: The authors declare no conflicts of interest.

References

1. Curl, R.F.; Capasso, F.; Gmachl, C.; Kosterev, A.A.; McManus, B.; Lewicki, R.; Pusharsky, M.; Wysocki, G.; Tittel, F.K. Quantum cascade lasers in chemical physics. *Chem. Phys. Lett.* **2010**, *487*, 1–18. [CrossRef]

2. Menzel, L.; Kosterev, A.; Curl, R.; Tittel, F.K.; Gmachl, C.; Capasso, F.; Sivco, D.; Baillargeon, J.; Hutchinson, A.; Cho, A.; et al. Spectroscopic detection of biological NO with a quantum cascade laser. *Appl. Phys. A* **2001**, *72*, 859–863. [CrossRef] [PubMed]
3. Schwaighofer, A.; Brandstetter, M.; Lendl, B. Quantum cascade lasers (QCLs) in biomedical spectroscopy. *Chem. Soc. Rev.* **2017**, *46*, 5903–5924. [CrossRef] [PubMed]
4. Elia, A.; Di Franco, C.; Spagnolo, V.; Lugarà, P.M.; Scamarcio, G. Quantum Cascade Laser-Based Photoacoustic Sensor for Trace Detection of Formaldehyde Gas. *Sensors* **2009**, *9*, 2697–2705. [CrossRef]
5. Lundqvist, S.; Kluczynski, P.; Weih, R.; Von Edlinger, M.; Nähle, L.; Fischer, M.; Bauer, A.; Höfling, S.; Koeth, J. Sensing of formaldehyde using a distributed feedback interband cascade laser emitting around 3493 nm. *Appl. Opt.* **2012**, *51*, 6009–6013. [CrossRef]
6. Kosterev, A.A.; Tittel, F.K. Chemical sensors based on quantum cascade lasers. *IEEE J. Quantum Electron.* **2002**, *38*, 582–591. [CrossRef]
7. Bugajski, M.; Pierściński, K.; Pierścińska, D.; Szerling, A.; Kosiel, K. Multimode instabilities in mid-infrared quantum cascade lasers. *Photonics Lett. Pol.* **2013**, *5*, 85–87. [CrossRef]
8. Faist, J.; Gmachl, C.; Capasso, F.; Sirtori, C.; Sivco, D.L.; Baillargeon, J.N.; Cho, A.Y. Distributed feedback quantum cascade lasers. *Appl. Phys. Lett.* **1997**, *70*, 2670–2672. [CrossRef]
9. Schartner, S.; Austerer, M.; Schrenk, W.; Andrews, A.M.; Klang, P.; Strasser, G. Surface emission from episide-down short distributed-feedback quantum cascade lasers. *Opt. Express* **2008**, *16*, 11920–11929. [CrossRef]
10. Hugi, A.; Maulini, R.; Faist, J. External cavity quantum cascade laser. *Semicond. Sci. Technol.* **2010**, *25*, 83001. [CrossRef]
11. Höfling, S.; Reithmaier, J.; Forchel, A. Device performance and wavelength tuning behavior of ultra-short quantum-cascade microlasers with deeply etched Bragg-mirrors. *IEEE J. Sel. Top. Quantum Electron.* **2005**, *11*, 1048–1054. [CrossRef]
12. Fuchs, P.; Friedl, J.; Höfling, S.; Koeth, J.; Forchel, A.; Worschech, L.; Kamp, M. Single mode quantum cascade lasers with shallow-etched distributed Bragg reflector. *Opt. Express* **2012**, *20*, 3890–3897. [CrossRef]
13. Colombelli, R.; Srinivasan, K.; Troccoli, M.; Painter, O.; Gmachl, C.; Tennant, D.M.; Sergent, A.M.; Sivco, D.L.; Cho, A.Y.; Capasso, F. Quantum Cascade Surface-Emitting Photonic Crystal Laser. *Science* **2003**, *302*, 1374–1377. [CrossRef] [PubMed]
14. Hugi, A.; Terazzi, R.; Bonetti, Y.; Wittmann, A.; Fischer, M.; Beck, M.; Faist, J.; Gini, E. External cavity quantum cascade laser tunable from 7.6 to 11.4 µm. *Appl. Phys. Lett.* **2009**, *95*, 61103. [CrossRef]
15. Coldren, L.A. Monolithic two-section GaInAsP/InP active-optical-resonator devices formed by reactive ion etching. *Appl. Phys. Lett.* **1981**, *38*, 315–317. [CrossRef]
16. Coldren, L.; Koch, T. Analysis and design of coupled-cavity lasers—Part I: Threshold gain analysis and design guidelines. *IEEE J. Quantum Electron.* **1984**, *20*, 659–670. [CrossRef]
17. Coldren, L.; Koch, T. Analysis and design of coupled-cavity lasers—Part II: Transient analysis. *IEEE J. Quantum Electron.* **1984**, *20*, 671–682. [CrossRef]
18. Höfling, S.; Heinrich, J.; Reithmaier, J.P.; Forchel, A.; Seufert, J.; Fischer, M.; Koeth, J. Widely tunable single-mode quantum cascade lasers with two monolithically coupled Fabry-Pérot cavities. *Appl. Phys. Lett.* **2006**, *89*, 241126. [CrossRef]
19. Li, H.; Manceau, J.-M.; Andronico, A.; Jagtap, V.; Sirtori, C.; Li, L.H.; Linfield, E.H.; Davies, G.; Barbieri, S. Coupled-cavity terahertz quantum cascade lasers for single mode operation. *Appl. Phys. Lett.* **2014**, *104*, 241102. [CrossRef]
20. Kundu, I.; Dean, P.; Valavanis, A.; Chen, L.; Li, L.H.; Cunningham, J.; Linfield, E.H.; Davies, G. Discrete Vernier tuning in terahertz quantum cascade lasers using coupled cavities. *Opt. Express* **2014**, *22*, 16595–16605. [CrossRef]
21. Giehler, M.; Kostial, H.; Hey, R.; Grahn, H. Suppression of longitudinal modes in two-sectioned, coupled-cavity GaAs/(Al,Ga) As terahertz quantum-cascade lasers. *Appl. Phys. Lett.* **2007**, *91*, 161102. [CrossRef]
22. Pierściński, K.; Pierścińska, D.; Pluska, M.; Gutowski, P.; Sankowska, I.; Karbownik, P.; Czerwinski, A.; Bugajski, M. Room temperature, single mode emission from two-section coupled cavity InGaAs/AlGaAs/GaAs quantum cascade laser. *J. Appl. Phys.* **2015**, *118*, 133103. [CrossRef]
23. Czerwinski, A.; Pluska, M.; Łaszcz, A.; Ratajczak, J.; Pierściński, K.; Pierścińska, D.; Gutowski, P.; Karbownik, P.; Bugajski, M. Formation of coupled-cavities in quantum cascade lasers using focused ion beam milling. *Microelectron. Reliab.* **2015**, *55*, 2142–2146. [CrossRef]

24. Pierściński, K.; Bugajski, M.; Czyszanowski, T.; Kolek, A.; Wesołowski, M.; Kuc, M.; Sarzała, R.P.; Dems, M.; Płuska, M.; Pierścińska, D.; et al. Coupled-cavity AlInAs/InGaAs/InP quantum cascade lasers fabricated by focused ion beam processing. *J. Phys. Photonics* **2018**, *1*, 015001. [CrossRef]
25. Bugajski, M.; Gutowski, P.; Karbownik, P.; Trajnerowicz, A.; Pierściński, K.; Pierścińska, D.; Sankowska, I.; Kubacka-Traczyk, J.; Sakowicz, M. Room temperature AlInAs/InGaAs/inP quantum cascade lasers. *Photonics Lett. Pol.* **2014**, *6*, 142–144. [CrossRef]
26. Gutowski, P.; Sankowska, I.; Słupiński, T.; Pierścińska, D.; Pierściński, K.; Kuźmicz, A.; Gołaszewska-Malec, K.; Bugajski, M. Optimization of MBE Growth Conditions of In0.52Al0.48As Waveguide Layers for InGaAs/InAlAs/InP Quantum Cascade Lasers. *Materials* **2019**, *12*, 1621. [CrossRef]
27. Bugajski, M.; Gutowski, P.; Karbownik, P.; Kolek, A.; Hałdaś, G.; Pierściński, K.; Pierścińska, D.; Kubacka-Traczyk, J.; Sankowska, I.; Trajnerowicz, A.; et al. Mid-IR quantum cascade lasers: Device technology and non-equilibrium Green's function modeling of electro-optical characteristics. *Phys. Status Solidi B* **2014**, *251*, 1144–1157. [CrossRef]
28. Bugajski MKosiel, K.; Szerling, A.; Kubacka-Traczyk, J.; Sankowska, I.; Karbownik, P.; Trajnerowicz, A.; Pruszynska-Karbownik, E.; Pierscinski, K.; Pierscinska, D. GaAs/AlGaAs (similar to 9.4 mu m) quantum cascade lasers operating at 260 K. *Bull. Pol. Acad. Sci. Tech. Sci.* **2010**, *58*, 471–476.
29. Pierścińska, D.; Pierściński, K.; Iwińska, M.; Kosiel, K.; Szerling, A.; Karbownik, P.; Bugajski, M. Electrical and optical characterization of mid-IR GaAs/AlGaAs quantum cascade lasers. *Proc. SPIE* **2012**, *8432*, 84321S.
30. Pierściński, K.; Pierścińska, D.; Szabra, D.; Nowakowski, M.; Wojtas, J.; Mikołajczyk, J.; Bielecki, Z.; Bugajski, M. Time resolved FTIR study of spectral tuning and thermal dynamics of mid-IR QCLs. *Proc. SPIE* **2014**, *9134*, 91341L.
31. Brandstetter, M.; Genner, A.; Schwarzer, C.; Mujagic, E.; Strasser, G.; Lendl, B. Time-resolved spectral characterization of ring cavity surface emitting and ridge-type distributed feedback quantum cascade lasers by step-scan FT-IR spectroscopy. *Opt. Express* **2014**, *22*, 2656–2664. [CrossRef]
32. Hempel, M.; Roben, B.; Schrottke, L.; Hübers, H.-W.; Grahn, H.T. Fast continuous tuning of terahertz quantum-cascade lasers by rear-facet illumination. *Appl. Phys. Lett.* **2016**, *108*, 191106. [CrossRef]
33. Kundu, I.; Dean, P.; Valavanis, A.; Chen, L.; Li, L.H.; Cunningham, J.; Linfield, E.H.; Davies, G. Quasi-continuous frequency tunable terahertz quantum cascade lasers with coupled cavity and integrated photonic lattice. *Opt. Express* **2017**, *25*, 486–496. [CrossRef]